Crystal and magnetic structures of $NdBaCo_2O_{5+\delta}$ ($\delta \sim 0.75$): A neutron diffraction study

D. D. Khalyavin*
Institute of Solid State and Semiconductors Physics, National Academy of Sciences, P. Brovka Street 17, 220072 Minsk, Belarus

O. Prokhnenko, N. Stüßer, and V. Sikolenko
Hahn-Meitner-Institut, Glienicker Straße 100, Berlin D-14109, Germany

V. Efimov
Joint Institute for Nuclear Research, 141980 Dubna, Russia

A. N. Salak, A. A. Yaremchenko, and V. V. Kharton
Department of Ceramics and Glass Engineering, CICECO, University of Aveiro, 3810-193 Aveiro, Portugal
(Received 16 January 2008; published 9 May 2008)

The crystal structure and magnetic ordering in $NdBaCo_2O_{5+\delta}$ cobaltites have been studied by neutron powder diffraction. A successful refinement of the high temperature paramagnetic patterns for both as-prepared ($\delta \sim 0.71$) and oxidized ($\delta \sim 0.75$) compositions was performed in the *Pmmm* space group with a $2a_p \times 2a_p \times 2a_p$ unit cell. The symmetry relationships between this phase and other structural types observed in oxygen-deficient $LBaCo_2O_{5+\delta}$ perovskites are discussed. The analysis of the low-temperature diffraction data on oxidized $NdBaCo_2O_{5.75}$ requires to account for the magnetic contribution originating from both the Nd and the Co sublattices. These are ordered at $T_C \sim 180$ K and $T_N \sim 40$ K, respectively, with ferromagnetic coupling inside the sublattices and antiferromagnetic coupling between them. A comparison of the neutron diffraction and magnetization data leads to the conclusion that no uniform ferromagnetic ordering of the Co sublattice is developed and a moderate amount of small antiferromagnetic clusters exists below T_C.

DOI: 10.1103/PhysRevB.77.174417 PACS number(s): 75.50.Dd, 61.05.F−

I. INTRODUCTION

Oxygen-deficient $LBaCo_2O_{5+\delta}$ (L=Lanthanide or Y) layered perovskites demonstrate a complex structural chemistry and rich magnetic phase diagrams as a function of oxygen stoichiometry.[1–5] Several structural types related to distinct anion-ordering mechanisms within the $[LO_\delta]$ layers have been identified and explored. The ordering was found to have a crucial effect on physical properties by promoting abundant cooperative phenomena coupled with the charge, spin, and orbital degrees of freedom. The compositions with low and intermediate oxygen contents ($0 \leq \delta \leq 0.5$) have attracted much attention, resulting in the discovery of new complex types of electronic ordering.[6–14] This stimulates studies that are focused on the oxygen-rich part ($\delta > 0.5$) of the diagrams. The recent reports on oxygen-vacancy ordering in $PrBaCo_2O_{5.75}$ that forms a unique superstructure (Fig. 1) with a tetragonal $P4/mmm$ ($2a_p \times 2a_p \times 2a_p$) symmetry[15–17] have provoked additional interest in strongly oxidized $LBaCo_2O_{5+\delta}$.

The different superstructures formed in the oxygen-deficient $[LO_\delta]$ layers lead to different distributions of the CoO_6 octahedra and CoO_5 square pyramids in the defective perovskite lattice (Fig. 1). This fact, in combination with the ability of cobalt cations to adopt diverse spin configurations depending on the local crystal chemistry, enables a systematic analysis of the relationships between oxygen stoichiometry, structure, and properties. In particular, numerous cooperative phenomena related to localized electronic states, such as charge and spin-state ordering, were revealed in the compositions wherein ($\delta < 0.5$) and the average Co oxidation state is lower than 3+.[6–14] The $LBaCo_2^{3+}O_{5.5}$ cobaltites demonstrate a well-defined competition between the localized and delocalized states, resulting in metal-insulator phase transition at $T_{MI} \sim 340$ K. The presence of Co^{4+} at $\delta > 0.5$ should promote strong ferromagnetic interactions and delocalization, thus altering the magnetic ground state and changing electrical properties.

The present work was centered on structural and magnetic studies near the critical point $\delta = 0.75$, at which a new type of superstructure may be expected. As the oxidation of $LBaCo_2O_{5+\delta}$ containing relatively small rare-earth ions is difficult, perovskite with L=Nd was selected as the model system. $NdBaCo_2O_{5+\delta}$ was already investigated elsewhere,[18–23] but in all cases, the samples were synthesized in air and contained less than 5.75 oxygen atoms/f.u. Burley *et al.*[18] reported a pure antiferromagnetic ground state with the G-type spin ordered configuration for $NdBaCo_2O_{5.69}$ studied by neutron diffraction. The crystal structure was refined in the orthorhombic *Pmmm* ($a_p \times 2a_p \times 2a_p$) space group typical for $\delta = 0.5$.[18] Lobanovsky *et al.*[20] refined the $NdBaCo_2O_{5.72}$ neutron diffraction patterns in the same space group with an expanded ($2a_p \times 2a_p \times 2a_p$) unit cell; both antiferromagnetic and ferromagnetic contributions were observed and interpreted in favor of a canted antiferromagnetic structure. Our neutron-diffraction study demonstrates that an oxidized composition with $\delta \approx 0.75$ exhibits a ferromagnetic behavior below 180 K without any indication of an antiferromagnetic phase. The presence of clusters with local antiferromagnetic ordering can be revealed, however, by comparing the diffraction and magnetization data. The analysis of the crystal structure symmetry supported the formation of the orthorhombic *Pmmm* ($2a_p \times 2a_p \times 2a_p$), a common isotropy subgroup of both the *Pmmm* ($2a_p \times 2a_p \times 2a_p$) and the

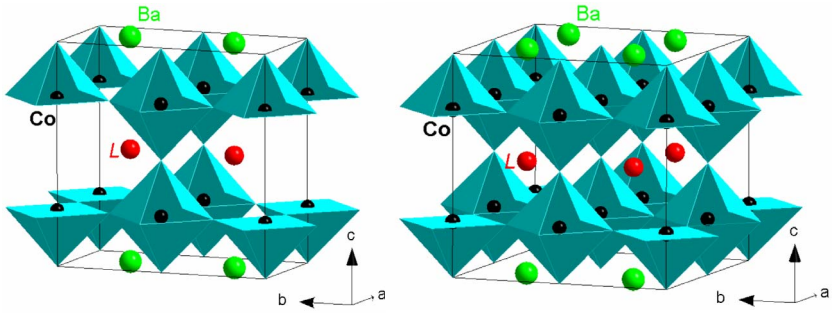

FIG. 1. (Color online) Schematic of the crystal structure for $L\mathrm{BaCo_2O_{5.5}}$, $Pmmm$ $(a_p \times 2a_p \times 2a_p)$ (left), and $L\mathrm{BaCo_2O_{5.75}}$, $P4/mmm$ $(2a_p \times 2a_p \times 2a_p)$ (right).

$P4/mmm$ $(2a_p \times 2a_p \times 2a_p)$ space groups, which allows continuous transformation between the corresponding structural types with $\delta=0.5$ and $\delta=0.75$.

II. EXPERIMENT

Samples of $\mathrm{NdBaCo_2O_{5+\delta}}$ with different oxygen contents were prepared by using a standard solid-state reaction method. The starting materials, namely, $\mathrm{Nd_2O_3}$ (99.99%, Aldrich), $\mathrm{BaCO_3}$ (99%, Merck), and $\mathrm{Co_3O_4}$ (99%, Aldrich), were mixed in an agate mortar and reacted at 1373 K for 10 h in air. The firing procedure and intermediate regrinding steps were repeated several times to remove impurity phases. Finally, the powder was cooled from 1373 K down to room temperature (2 K/min) in order to achieve equilibrium with atmospheric oxygen. Hereafter, this sample equilibrated in air is referred to as "as prepared." A series of powdered samples were then equilibrated in flowing oxygen (oxidized sample) or in an $(\mathrm{O_2}+\mathrm{N_2})$ mixture, wherein the oxygen partial pressure measured by using an electrochemical solid-electrolyte sensor was 52.3 kPa. The equilibration was performed at 923 K for 10 h; then, the samples were slowly cooled (2 K/min) down to room temperature in the same atmosphere. X-ray diffraction (XRD) analysis (Rigaku D/MAX-B diffractometer, Cu $K\alpha$ radiation) confirmed that all powders were single phase; the XRD patterns exhibited splitting of the fundamental perovskite multiplets (hkl; $k=l$) that is characteristic of the orthorhombic distortions.

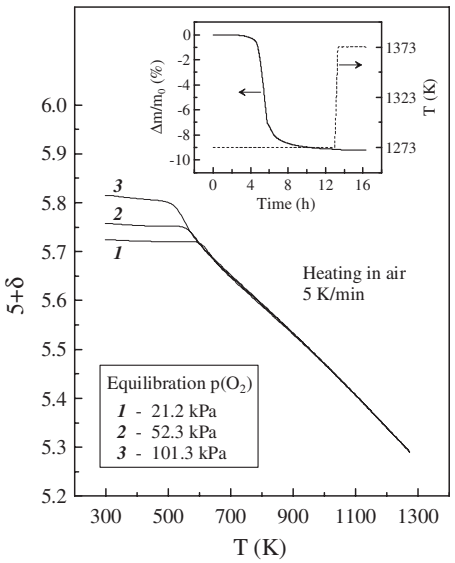

FIG. 2. Oxygen nonstoichiometry variations in $\mathrm{NdBaCo_2O_{5+\delta}}$ equilibrated at different oxygen partial pressures upon heating in air. The inset illustrates the relative weight changes of the $\mathrm{NdBaCo_2O_{5+\delta}}$ sample on reduction (see text).

Thermogravimetric analysis (TGA) was performed by using a Setaram Setsys 16/18 instrument in flowing dry air at a heating rate of 5 K/min, as shown in Fig. 2. The initial weight of the samples was ~0.6 g and the instrument sensitivity is 0.4 μg. In order to calculate the absolute values of the oxygen content $(5+\delta)$, the samples were equilibrated in air at 1273 K for 2 h, followed by flushing with pure Ar for 1 h and subsequent reduction in flowing 10% $\mathrm{H_2}$–90% $\mathrm{N_2}$ mixture for 12–14 h at 1273–1373 K. One example of the TGA curve collected on reduction is given in the inset of Fig. 2. The results of the oxygen content determination are summarized in Table I.

The dc magnetization was measured by using a superconducting quantum interface device magnetometer (Quantum Design, MPMS-5) in the temperature range of 5–300 K. The curve registered at 1 kOe after cooling in this field (FC) displays two critical temperatures, namely, $T_C \sim 180$ K and $T_N \sim 40$ K (Fig. 3), when the magnetization increases and decreases, respectively. The low-temperature field isotherms clearly demonstrated that the value of spontaneous magnetization becomes smaller below T_N, as illustrated in the inset of Fig. 3.

Neutron diffraction experiments were carried out in the Berlin Neutron Scattering Center (BENSC) at the Hahn-Meitner-Institute. Two powder diffractometers were used, namely, the fine-resolution powder diffractometer (E9) and the high-intensity focusing diffractometer (E6). The former, with incident neutrons of wavelength $\lambda=1.7974$ Å and resolution $\Delta d/d \sim 2\times10^{-3}$, was used for the crystal structure refinement. The second diffractometer ($\lambda=2.439$ Å), which

TABLE I. Oxygen content in $\mathrm{NdBaCo_2O_{5+\delta}}$ equilibrated in different atmospheres.

Oxygen partial pressure in the course of equilibration (kPa)	T (K)	$5+\delta$
21.2	298	5.724
	1273	5.287
52.3	298	5.757
101.3	298	5.815

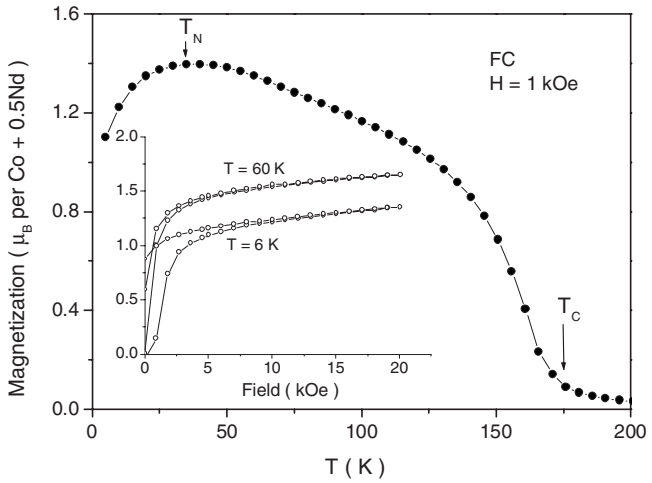

FIG. 3. Temperature dependence of magnetization registered on heating in $H=1$ kOe after cooling in this field. The inset shows the field dependences of magnetization at two temperatures.

is equipped with a position sensitive detector that provides a very high intensity, is efficient for the magnetic structure investigations. The obtained data were refined by the Rietveld method by using FULLPROF SUITE.[24] Group-theoretical calculations were performed with the aid of the ISOTROPY software.[25]

III. RESULTS AND DISCUSSION

A. Crystal structure

An inspection of the x-ray and high resolution neutron diffraction patterns revealed that both the oxidized and the as-prepared samples are characterized by an orthorhombic metric of the primitive perovskite unit cell (inset of Fig. 4), which is typical of $L\mathrm{BaCo_2O_{5.5}}$. At the same time, the splitting of the fundamental multiplets in the case of oxidized sample was very weak; the quality of the La Bail analysis[26] of the neutron diffraction data in the orthorhombic *Pmmm* space group was only slightly better than in tetragonal *P4/mmm*. The analysis of the XRD patterns of $\mathrm{NdBaCo_2O_{5+\delta}}$ with variable oxygen contents also lead to the conclusion that the orthorhombic distortions correlate with δ and can be gradually changed by varying the annealing conditions. This observation is consistent with the data on $\mathrm{PrBaCo_2O_{5+\delta}}$ in the range of $0.5<\delta<0.8$.[27] A question arises, however, if increasing the oxygen concentration may result in a gradual transformation of the orthorhombic *Pmmm* $(a_p\times 2a_p\times 2a_p)$ structure (122) characteristic for $\delta\sim 0.5$ into the tetragonal *P4/mmm* $(2a_p\times 2a_p\times 2a_p)$ structure (222) reported by Frontera *et al.*[15–17] for $\delta\sim 0.75$. As there is no group-subgroup relation between these structures, the direct *Pmmm* $(a_p\times 2a_p\times 2a_p)\rightarrow$ *P4/mmm* $(2a_p\times 2a_p\times 2a_p)$ transition must be discontinuous, which favors the formation of a phase mixture with different types of vacancy ordering. However, this transformation may also be a succession of two continuous transitions if there is an appropriate common subgroup. Examination of the isotropy subgroups of the *Pmmm* and *P4/mmm* space groups associated with the X $(\boldsymbol{k}=\boldsymbol{a}^*/2)$ and Γ $(\boldsymbol{k}=0)$ points, respectively, revealed that the *Pmmm* $(2a_p\times 2a_p\times 2a_p)$ subgroup appears twice: as a result of the *Pmmm* $(a_p\times 2a_p\times 2a_p)\rightarrow$ *Pmmm* $(2a_p\times 2a_p\times 2a_p)$ isomorphic phase transformation mediated by X_1^+ irreducible presentation, and as a *P4/mmm* $(2a_p\times 2a_p\times 2a_p)\rightarrow$ *Pmmm* $(2a_p\times 2a_p\times 2a_p)$ crossover associated with Γ_2^+ representation.[25] In both cases, continuous transitions are allowed in renormalization-group theory. Thus, the experimental data and symmetry consideration both argue in favor of an intermediate phase with *Pmmm* $(2a_p\times 2a_p\times 2a_p)$ symmetry. This intermediate phase was indeed recently reported by Lobanovky *et al.*[20,21] for $\mathrm{NdBaCo_2O_{5.72}}$.

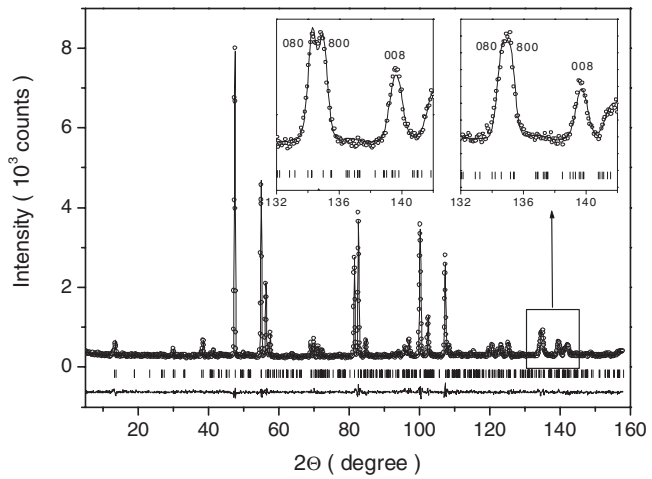

FIG. 4. The E9 neutron diffraction pattern ($\lambda=1.7974$ Å) of the oxidized $\mathrm{NdBaCo_2O_{5+\delta}}$ sample, collected at 295 K and refined in the *Pmmm* $(2a_p\times 2a_p\times 2a_p)$ space group. The inset shows the (800) fundamental multiplet illustrating a presence of orthorhombic distortions in both the oxidized (right panel) and the as-prepared (left panel) samples.

To discuss the mechanism of these compositionally driven structural transformations and resultant behavior of the unit cell distortions, one should consider Wyckoff positions mapping on the corresponding symmetry changes (Fig. 5). The oxygen positions in the $[\mathrm{NdO}_\delta]$ layer are crucial as they determine the distribution of pyramidally and octahedrally coordinated cobalt. In the ideal *P4/mmm* $(2a_p\times 2a_p\times 2a_p)$ structure, there are two occupied oxygen positions in this layer, namely $1d$ and $2e$. The first corresponds to $1h$ in the *Pmmm* $(2a_p\times 2a_p\times 2a_p)$ subgroup, while the second splits into two independent positions, which are $1g$ and $1d$. Therefore, the alterations in occupancy probability of these positions can be considered as a scalar order parameter for the *P4/mmm* $(2a_p\times 2a_p\times 2a_p)\rightarrow$ *Pmmm* $(2a_p\times 2a_p\times 2a_p)$ phase transition; different occupancies of the $1g$ and $1d$ sites should induce orthorhombic distortions. In an ideal case, one of the positions ($1g$ in Fig. 5) is always entirely occupied, whereas the occupancy probability for another site gradually decreases with reducing oxygen content and becomes zero in the *Pmmm* $(a_p\times 2a_p\times 2a_p)$ structure.

The validity of this scenario can be clearly demonstrated by the Fourier difference map obtained after the refinement of the neutron diffraction pattern for the as-prepared sample in the *Pmmm* $(2a_p\times 2a_p\times 2a_p)$ space group with disordered oxygen vacancies over the four independent oxygen posi-

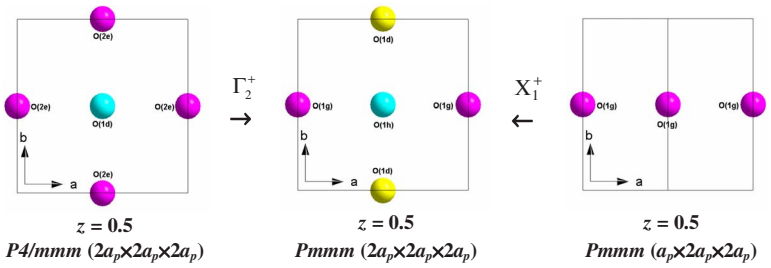

FIG. 5. (Color online) Splitting of oxygen positions in the $[NdO_\delta]$ layer at the $P4/mmm$ $(2a_p \times 2a_p \times 2a_p) \rightarrow Pmmm$ $(2a_p \times 2a_p \times 2a_p)$ and $Pmmm$ $(a_p \times 2a_p \times 2a_p) \rightarrow Pmmm$ $(2a_p \times 2a_p \times 2a_p)$ phase transitions. The O(1*d*) and O(1*g*) positions in the $Pmmm$ $(2a_p \times 2a_p \times 2a_p)$ subgroup are characterized with different occupancy probabilities.

tions in the $[NdO_\delta]$ layer (Fig. 6). The map exhibits two pronounced negative peaks having nonequivalent residual densities with (0,0,0.5) and (0.5,0,0.5) coordinates, which correspond to the 1*c* and 1*d* positions. On the contrary, there is no substantial density fluctuation in the (0,0.5,0.5) point, indicating that the average occupancy is quite close to the actual occupancy of the 1*g* site. The positive residual density at (0.5,0.5,0.5) testifies that the occupancy of 1*h* position is essentially complete. The occupancy probability for the 1*g* position is thus larger than that for 1*d*, which is in agreement with the refined $a < b$ ratio.

By taking into account these relationships, the neutron diffraction patterns for both oxidized and as-prepared samples were refined in the $Pmmm$ $(2a_p \times 2a_p \times 2a_p)$ space group. The structural parameters are summarized in Table II; the fitting quality is illustrated by Fig. 4. The accuracy of the oxygen content estimation was low owing to large standard deviations for the 1*c*, 1*d*, 1*s*, and 1*h* site occupancies. The complexity of this structure involving 12 distinct oxygen positions decreases the statistic weight of separate sites. In order to increase accuracy, the crystal structure of the oxidized sample was approximated by using a simple tetragonal model ($P4/mmm$, $a_p \times a_p \times 2a_p$) that accounts only for the Nd/Ba cation ordering. This approximation is possible due to pseudotetragonal metric and very low intensity of the reflections, which originate from the oxygen-vacancy ordering in $[NdO_\delta]$ layers and require expansion of the primitive perovskite unit cell. The simple tetragonal model comprises only three independent oxygen positions: O1(1*a*), O2(4*i*), and O3(1*b*). The results displayed that the 1*a* and 4*i* sites are completely occupied, confirming that all vacancies are located in the 1*b* position ($[NdO_\delta]$ layer). For the latter position, the occupancy factor was 0.763(8), giving an oxygen content of 5.76 ± 0.02 atom/f.u. with a 99% confidence probability. A discrepancy of this value with the TGA result (Table I), is apparently, can be addressed to the factors discussed by Conder *et al.*[28] These authors found that thermogravimetric hydrogen reduction sometimes gives an overestimation of oxygen content in $LBaCo_2O_{5+\delta}$ cobaltites in comparison to the iodometric titration and gas volumetric analysis.

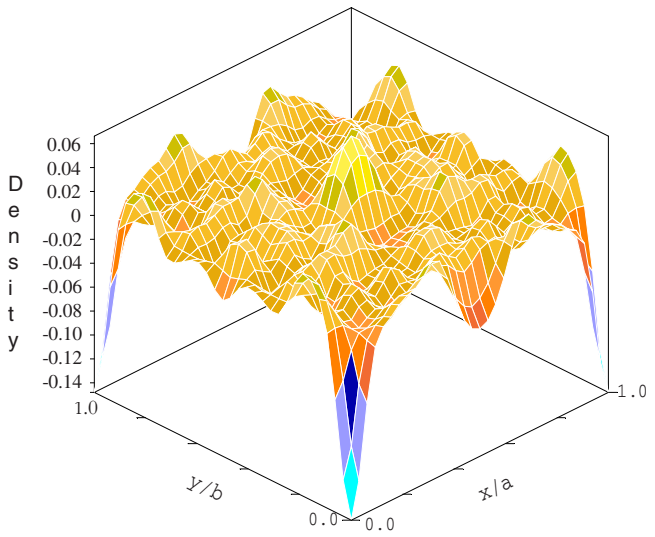

FIG. 6. (Color online) 3D Fourier difference map (z=0.5) calculated after the refinement of the neutron diffraction pattern for the as-prepared $NdBaCo_2O_{5+\delta}$ sample in the $Pmmm$ $(2a_p \times 2a_p \times 2a_p)$ space group, with disordered oxygen vacancies over the apical oxygen positions in the $[NdO_\delta]$ layer (1*c*, 1*d*, 1*g* and 1*h* positions).

Thus, the result of the refinement indicates that the oxidized composition is close to the critical point δ=0.75. In spite of this fact, its symmetry is definitely orthorhombic, suggesting that the tetragonal $P4/mmm$ $(2a_p \times 2a_p \times 2a_p)$ structure is not stable even in these conditions. The structural parameters (Table II) show that the 1*c* position, which should be entirely empty in the ideal 222 structure, is partially occupied in the studied samples. Apparently, the "mixture degrees" of this position with 1*e* and 1*d* are not equivalent. In other words, the oxygen ions present in the 1*c* position appear to mainly come from either 1*g* or 1*d* sites, leading to different occupancy of these positions, and consequently, to breakdown of the tetragonal symmetry.

B. Magnetic structure

In agreement with the magnetization data (Fig. 3), additional contribution to nuclear reflections can be clearly observed in the E6 diffraction patterns of the oxidized sample below $T_C \sim 180$ K (Fig. 7). This contribution can be accounted in the refinement by introducing the ferromagnetic component localized on the Co positions. The refinement quality was found rather sensitive to the magnetic moment direction, allowing a rough quantitative evaluation (Fig. 8). The basic components that transform according to different irreducible representations (irreps) of the $\boldsymbol{k}=0$ wave vector group and enter the global magnetic representation D_m on the Co positions

$$D_m = \Gamma_2^+ + \Gamma_3^+ + \Gamma_4^+ + \Gamma_1^- + \Gamma_3^- + \Gamma_4^- \quad (1)$$

are presented in Table III. Note that the magnetic representation is the same for all 2*q*, 2*s*, 2*r*, and 2*t* Co sites. By using the basis functions of a single irrep, the best magnetic *R*

TABLE II. Atomic positions (x,y,z), isotropic temperature factors (B), and site occupancies for the $NdBaCo_2O_{5+\delta}$ structure, which are refined in the *Pmmm* space group by using the high-resolution powder neutron diffraction collected at room temperature. The unit cell parameters and reliability factors for the oxidized sample (left) are $a=7.7772(2)$ Å, $b=7.7934(2)$ Å, $c=7.6139(2)$ Å, $R_p=4.95\%$, $R_{wp}=6.42\%$, and $\chi^2=1.59$ and for the as-prepared sample (right), $a=7.7825(2)$ Å, $b=7.8023(2)$ Å, $c=7.6074(2)$ Å, $R_p=3.77\%$, $R_{wp}=4.92\%$, and $\chi^2=2.29$.

Atom	Wyck	x	y	z	B	Occup.	x	y	z	B	Occup.
Ba	4*y*	0.250(3)	0.249(3)	0	0.9(1)	1	0.252(2)	0.253(2)	0	0.02(8)	1
Nd	4*z*	0.254(2)	0.252(3)	0.5	0.2(1)	1	0.2600(8)	0.255(1)	0.5	0.41(8)	1
Co_{Py}	2*q*	0	0	0.246(8)	0.6(1)	1	0	0	0.244(4)	0.23(9)	1
Co_{Oc1}	2*t*	0.5	0.5	0.253(8)	0.6(1)	1	0.5	0.5	0.243(3)	0.23(9)	1
Co_{Oc2}	2*r*	0	0.5	0.259(5)	0.6(1)	1	0	0.5	0.257(5)	0.23(9)	1
Co_{Oc3}	2*s*	0.5	0	0.242(6)	0.6(1)	1	0.5	0	0.253(5)	0.23(9)	1
O1	1*a*	0	0	0	1.2(1)	1	0	0	0	0.67(8)	1
O2	1*b*	0.5	0	0	1.2(1)	1	0.5	0	0	0.67(8)	1
O3	1*c*	0	0	0.5	0.6(2)	0.31(3)	0	0	0.5	0.7(1)	0.22(3)
O4	1*d*	0.5	0	0.5	0.6(2)	0.93(3)	0.5	0	0.5	0.7(1)	0.79(3)
O5	1*e*	0	0.5	0	1.2(2)	1	0	0.5	0	0.67(8)	1
O6	1*f*	0.5	0.5	0	1.2(2)	1	0.5	0.5	0	0.67(8)	1
O7	1*g*	0	0.5	0.5	0.6(2)	0.93(3)	0	0.5	0.5	0.7(1)	0.84(4)
O8	1*h*	0.5	0.5	0.5	0.6(2)	0.88(4)	0.5	0.5	0.5	0.7(1)	0.99(3)
O9	4*u*	0	0.756(5)	0.716(2)	1.9(3)	1	0	0.747(3)	0.707(1)	0.8(2)	1
O10	4*v*	0.5	0.753(5)	0.736(1)	1.2(2)	1	0.5	0.747(3)	0.724(1)	0.3(1)	1
O11	4*w*	0.249(5)	0	0.717(4)	0.9(3)	1	0.249(4)	0	0.717(2)	1.2(2)	1
O12	4*x*	0.249(5)	0.5	0.716(4)	0.8(3)	1	0.244(4)	0.5	0.732(2)	2.2(3)	1

factor was obtained in the model wherein magnetic moments are directed along the *a* axis (Fig. 8, Γ_3^+ irrep). However, the refinement quality can be substantially improved by mixing the ferromagnetic components, transforming as basis functions of the three different irreps $(\Gamma_2^+ + \Gamma_3^+ + \Gamma_1^+)$. Due to the angular degeneracy of the exchange energy, these irreps form an exchange multiplet corresponding to a single irreducible

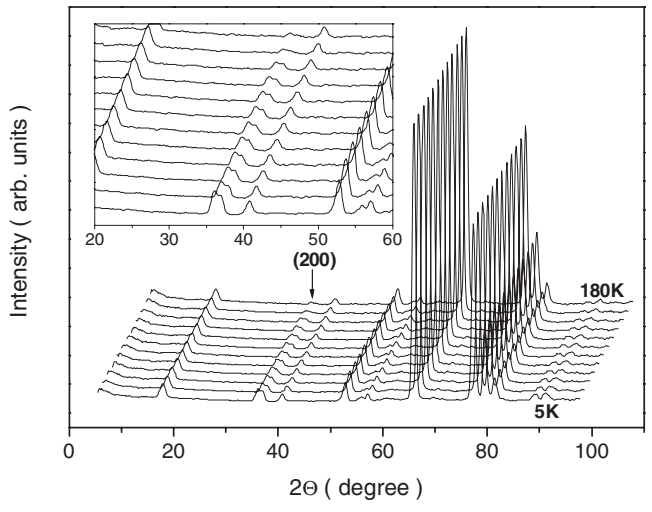

FIG. 7. Neutron diffraction patterns of the oxidized $NdBaCo_2O_{5+\delta}$ sample collected on the E6 diffractometer in the temperature range of 5–180 K. The inset presents an expanded view near the (200) fundamental multiplet, wherein ferromagnetic contribution is well defined.

representation of the exchange Hamiltonian. This indicates that the magnetocrystalline anisotropy splitting different components of the exchange multiplets is negligibly small compared to the exchange interactions. Note that the 122 compounds, wherein the oxygen content is close to 5.5, exhibit the Ising-type spin anisotropy.[29–35]

As the diffraction patterns do not allow separate determinations of the four independent Co positions, the magnetic intensity was fitted by assuming equal values of their magnetic moments. Moreover, only Γ_2^+ and Γ_3^+ irreps were mixed during refinement in order to decrease the standard deviation of the total moment and the corresponding components. Due to the small difference between the *a* and *b* parameters (the metric is close to tetragonal), it is impossible to determine the mixing coefficients for Γ_3^+ and Γ_4^+ irreps; the direction of magnetic moments in the (*ab*) plane was, hence, arbitrarily fixed along the *a* axis. With these restrictions, the value of the *c* component was always statistically significant at temperatures lower than 140 K and the moment direction in the (*ac*) plane was temperature independent within the limits of experimental error.

The magnetic phase described above does not provide a satisfactory fitting quality for the diffraction patterns recorded at temperatures below $T_N \sim 40$ K. A comparison of the patterns that are collected at 5 and 40 K (Fig. 9) displays significant changes that cannot be attributed to the spin-wave processes related to different temperatures. One important feature is the contribution to the nuclear reflections with *h*, $k=2n$; $l=2n+1$, pointing to *c*-directional modulation. These scattering alterations correlate with the decreasing spontane-

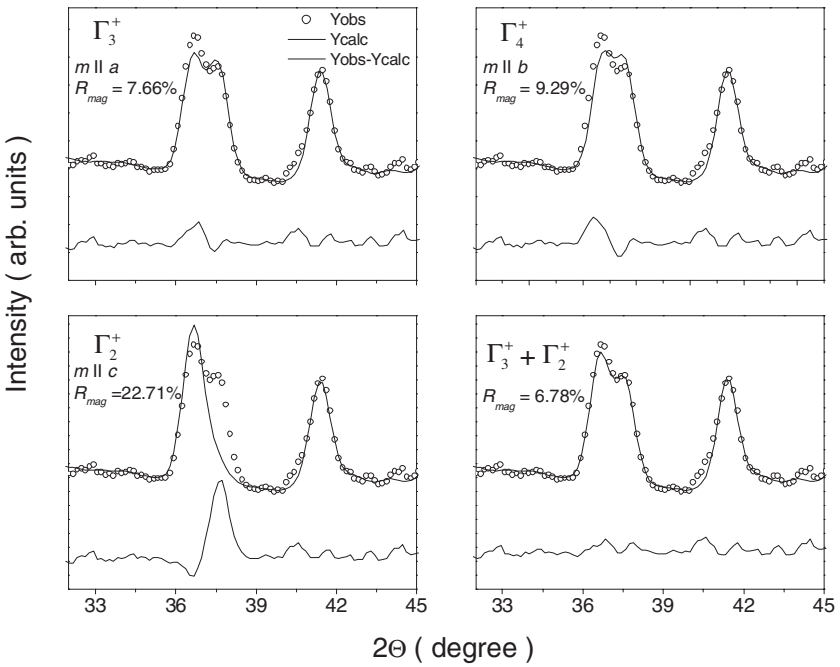

FIG. 8. Fragment of the E6 neutron diffraction pattern of the oxidized $NdBaCo_2O_{5+\delta}$ sample near the (200) fundamental multiplet, which is taken at 60 K and refined by using the models with different orientation of the Co magnetic moment *m*.

ous magnetization revealed by the magnetic measurements (Fig. 3). The most logical explanation relates to a gradual polarization of the Nd sublattice caused by negative *f-d* exchange. Interchanging of the *c* planes populated by paramagnetic Nd^{3+} and diamagnetic Ba^{2+} should naturally introduce magnetic modulation along this direction. A successful refinement of the neutron diffraction patterns by using the model involving two sublattices provided a quantitative validation of this hypothesis (Fig. 9). The magnetic representation for the 4*x* Wyckoff position occupied by Nd can be decomposed as

$$D_m = \Gamma_1^+ + \Gamma_2^+ + 2\Gamma_3^+ + 2\Gamma_4^+ + 2\Gamma_1^- + 2\Gamma_2^- + \Gamma_3^- + \Gamma_4^-, \quad (2)$$

with the corresponding basis functions listed in Table III. Again, two irreps Γ_2^+ and Γ_3^+ were used to refine this sublattice. At 5 K, the calculated magnetic moments for Nd and Co cations are $1.35(5)\mu_B$ and $1.52(3)\mu_B$, respectively. The directions of these sublattices were found opposite to each other within the limits of experimental uncertainty. The resultant ferrimagnetic model is schematically shown in the inset of Fig. 10. This model is in satisfactory agreement with the low-temperature magnetic measurements wherein the uncompensated moment of $\sim 1\mu_B/(\mathrm{Co}+0.5\mathrm{Nd})$ was obtained at 5 K. The temperature dependence of the magnetic moment of Co ions evaluated from the neutron diffraction data is presented in Fig. 10. The behavior is typical for ferromagnetics with the estimated Curie temperature $T_C \sim 180$ K. On the other hand, the behavior of the oxidized $NBaCo_2O_{5+\delta}$ cannot be considered as classical ferromagnetic even in the temperature range wherein the contribution of Nd sublattice

TABLE III. Atomic components of basis functions (*S*) of irreducible representations of the *Pmmm* space group for the Nd and Co positions. $4z-1(x,y,1/2)$, $2(x,-y,-1/2)$, $3(-x,y,-1/2)$, and $4(-x,-y,1/2)$; $2q-1(0,0,z)$, $2(0,0,-z)$; $2s-1(1/2,0,z)$, $2(1/2,0,-z)$; $2r-1(0,1/2,z)$, $2(0,-1/2,-z)$; $2t-1(1/2,1/2,z)$, and $2(1/2,-1/2,-z)$.

Irrep (mode)		Γ_1^+			Γ_2^+			Γ_3^+ (1)			Γ_3^+ (2)			Γ_4^+ (1)			Γ_4^+ (2)			Γ_1^- (1)			Γ_1^- (2)			Γ_2^- (1)			Γ_2^- (2)			Γ_3^-			Γ_4^-		
Projection		S_x	S_y	S_z	S_x	S_y	S_z	S_x	S_y	S_z	S_x	S_y	S_z	S_x	S_y	S_z	S_x	S_y	S_z	S_x	S_y	S_z	S_x	S_y	S_z	S_x	S_y	S_z	S_x	S_y	S_z	S_x	S_y	S_z	S_x	S_y	S_z
Wyckoff	1	0	0	1	0	0	1	1	0	0	0	1	0	1	0	0	0	1	0	1	0	0	0	1	0	1	0	0	0	1	0	0	0	1	0	0	1
$4z$	2	0	0	$\bar{1}$	0	0	1	1	0	0	0	$\bar{1}$	0	$\bar{1}$	0	0	0	1	0	1	0	0	0	$\bar{1}$	0	$\bar{1}$	0	0	0	1	0	0	0	$\bar{1}$	0	0	1
	3	0	0	$\bar{1}$	0	0	1	1	0	0	0	$\bar{1}$	0	$\bar{1}$	0	0	0	1	0	$\bar{1}$	0	0	0	1	0	1	0	0	0	$\bar{1}$	0	0	0	1	0	0	$\bar{1}$
	4	0	0	1	0	0	1	1	0	0	0	1	0	1	0	0	0	1	0	$\bar{1}$	0	0	0	$\bar{1}$	0	$\bar{1}$	0	0	0	$\bar{1}$	0	0	0	$\bar{1}$	0	0	$\bar{1}$
Wyckoff	1				0	0	1	1	0	0				0	1	0				0	0	1										0	1	0	1	0	0
$2q$	2				0	0	1	1	0	0				0	1	0				0	0	$\bar{1}$										0	$\bar{1}$	0	$\bar{1}$	0	0
Wyckoff	1				0	0	1	1	0	0				0	1	0				0	0	1										0	1	0	1	0	0
$2r$	2				0	0	1	1	0	0				0	1	0				0	0	$\bar{1}$										0	$\bar{1}$	0	$\bar{1}$	0	0
Wyckoff	1				0	0	1	1	0	0				0	1	0				0	0	1										0	1	0	1	0	0
$2s$	2				0	0	1	1	0	0				0	1	0				0	0	$\bar{1}$										0	$\bar{1}$	0	$\bar{1}$	0	0
Wyckoff	1				0	0	1	1	0	0				0	1	0				0	0	1										0	1	0	1	0	0
$2t$	2				0	0	1	1	0	0				0	1	0				0	0	$\bar{1}$										0	$\bar{1}$	0	$\bar{1}$	0	0

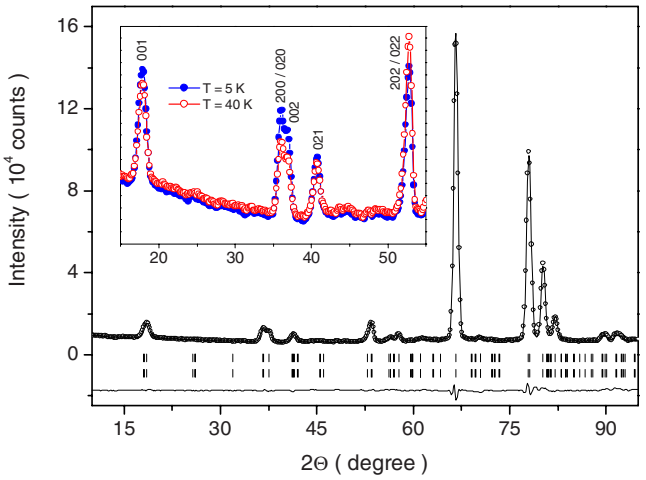

FIG. 9. (Color online) The refined E6 diffraction pattern ($\lambda = 2.439$ Å) of the oxidized $NdBaCo_2O_{5+\delta}$ sample, which is collected at 5 K. The inset compares fragments of two patterns recorded at different temperatures (see text).

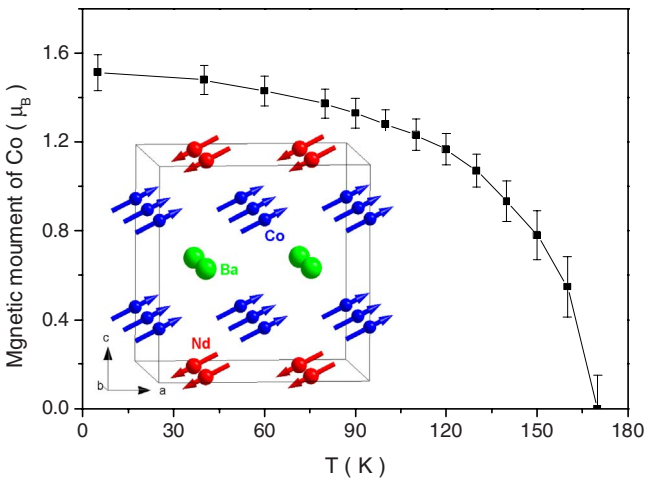

FIG. 10. (Color online) Temperature dependence of the averaged magnetic moment of Co ions, which is calculated from the refinement results of the E6 neutron diffraction patters. The inset shows schematic representation of the low temperature magnetic structure of the oxidized $NdBaCo_2O_{5+\delta}$ sample where the Nd and Co sublattices are both ordered.

is negligible ($T > T_N$). The saturated magnetic moment of Co sublattice is considerably lower than the value expected from the effective paramagnetic moment (μ_{eff}) estimated from the magnetic data. The inverse paramagnetic susceptibility at 190–300 K yields the μ_{eff} value of $3.72\mu_B$/Co after subtracting the Nd contribution. This corresponds to predominant high- and low-spin states for Co^{3+} ($t_{2g}^4 e_g^2$, $S=2$) and Co^{4+} ($t_{2g}^5 e_g^0$, $S=1/2$), respectively. Such a mismatch suggests a nonhomogeneous low temperature magnetic state, which can be associated with increasing population of the low-spin diamagnetic Co^{3+} ($t_{2g}^6 e_g^0$, $S=0$) ions at temperatures below T_C and with presence of small antiferromagnetic clusters. The cluster size and volume fraction is related to the Co^{4+} concentration, i.e., to the total oxygen content. When δ decreases, the clusters rapidly grow, reaching the neutron-diffraction coherence length in the composition equilibrated with atmospheric oxygen.[21] Although the antiferromagnetic contribution in the neutron diffraction patterns of as-prepared samples was also ascribed to a possible canting structure,[21] the scenario with two magnetic phases seems more likely because of the symmetry constraints [Eq. (1) and Table III] forbidding a noncollinear ordering of the Co sublattice. Besides, a nonhomogeneous magnetic state was found in many perovskite oxides containing cobalt ions in mixed valence state.[36–38]

IV. CONCLUSIONS

$NdBaCo_2O_{5+\delta}$ cobaltite with $\delta \approx 0.75$ possesses the orthorhombic $Pmmm$ ($2a_p \times 2a_p \times 2a_p$) symmetry, a common subgroup for the $Pmmm$ ($a_p \times 2a_p \times 2a_p$) and $P4/mmm$ ($2a_p \times 2a_p \times 2a_p$) space groups describing the symmetry of 122 and 222 structural types, respectively. This group-subgroup relation allows a continuous transformation of the 122 structure into the 222 polymorph via two successive second-order phase transitions induced by the oxygen content variations. Although a long-range ferromagnetic order in the Co sublattice is established below $T_C \sim 180$ K, the ferromagnetic state is not uniform due to the existence of antiferromagnetically ordered clusters, which are smaller than the neutron diffraction coherence length. At low temperatures $T < T_N \sim 40$ K, a negative f-d exchange polarizes the Nd sublattice in the direction opposite to the cobalt sublattice, forming an overall ferrimagnetic structure. The magnetic moments are characterized with the values of $1.52(3)\mu_B$ for Co and $1.35(5)\mu_B$ for Nd cations at 5 K.

ACKNOWLEDGMENTS

The neutron diffraction experiment at BENSC was supported by the European Commission under the 6th Framework Programme through the Key Action: Strengthening the European Research Area, Research Infrastructures, Contract No. RII3-CT-2003-505925 (NMI3). This work was also partially supported by the Russian Foundation for Basic Research (Grant No. 08-02-90053-Bel_a) and by the FCT, Portugal (Project No. PTDC/CTM/64357/2006).

*Author to whom correspondence should be addressed; khalyav@ifttp.bas-net.by

[1] W. Zhou, C. T. Lin, and W. Y. Liang, Adv. Mater. (Weinheim, Ger.) **5**, 735 (1993).
[2] W. Zhou, Chem. Mater. **6**, 441 (1994).
[3] C. Martin, A. Maignan, D. Pelloquin, N. Nguyen, and B. Raveau, Appl. Phys. Lett. **71**, 1421 (1997).
[4] A. Maignan, C. Martin, D. Pelloquin, N. Nguyen, and B. Raveau, J. Solid State Chem. **142**, 247 (1999).
[5] D. Akahoshi and Y. Ueda, J. Solid State Chem. **156**, 355 (2001).
[6] E. Suard, F. Fauth, V. Caignaert, I. Mirebeau, and G. Baldinozzi, Phys. Rev. B **61**, R11871 (2000).
[7] F. Fauth, E. Suard, V. Caignaert, B. Domenges, I. Mirebeau, and L. Keller, Eur. Phys. J. B **21**, 163 (2001).
[8] T. Vogt, P. M. Woodward, P. Karen, B. A. Hunter, P. Henning, and A. R. Moodenbaugh, Phys. Rev. Lett. **84**, 2969 (2000).
[9] F. Fauth, E. Suard, V. Caignaert, and I. Mirebeau, Phys. Rev. B **66**, 184421 (2002).
[10] Yu. P. Chernenkov, V. P. Plakhty, V. I. Fedorov, S. N. Barilo, S. V. Shiryaev, and G. L. Bychkov, Phys. Rev. B **71**, 184105 (2005).
[11] V. P. Plakhty, Y. P. Chernenkov, S. N. Barilo, A. Podlesnyak, E. Pomjakushina, E. V. Moskvin, and S. V. Gavrilov, Phys. Rev. B **71**, 214407 (2005).
[12] Yu. P. Chernenkov, V. P. Plakhty, A. G. Gukasov, S. N. Barilo, S. V. Shiryaev, G. L. Bychkov, V. Hinkov, V. I. Fedorov, and V. A. Chekanov, Phys. Lett. A **365**, 166 (2007).
[13] D. D. Khalyavin, Phys. Rev. B **72**, 134408 (2005).
[14] D. D. Khalyavin, D. N. Argyriou, U. Amann, A. A. Yaremchenko, and V. V. Kharton, Phys. Rev. B **75**, 134407 (2007).
[15] C. Frontera, J. L. Garcia-Munoz, A. E. Carrillo, C. Ritter, D. Martiny Marero, and A. Caneiro, Phys. Rev. B **70**, 184428 (2004).
[16] C. Frontera, J. L. Garcia-Munoz, A. E. Carrillo, A. Caneiro, C. Ritter, and D. M. Y. Marero, J. Appl. Phys. **97**, 10C106 (2005).
[17] C. Frontera, A. Caneiro, A. E. Carrillo, J. Oro-Sole, and J. L. Garcia-Munoz, Chem. Mater. **17**, 5439 (2005).
[18] J. C. Burley, J. F. Mitchell, S. Short, D. Miller, and Y. Tang, J. Solid State Chem. **170**, 339 (2003).
[19] J. F. Mitchell, J. Burley, and S. Short, J. Appl. Phys. **93**, 7364 (2003).
[20] L. S. Lobanovsky, I. O. Troyanchuk, H. Szymczak, and O. Prokhnenko, J. Exp. Theor. Phys. **103**, 740 (2006).
[21] L. S. Lobanovskii and I. O. Troyanchuk, JETP Lett. **82**, 719 (2005).
[22] D. D. Khalyavin, I. O. Troyanchuk, N. V. Kasper, and H. Szymczak, J. Exp. Theor. Phys. **93**, 805 (2001).
[23] D. D. Khalyavin, A. P. Sazonov, I. O. Troyanchuk, R. Szymczak, and H. Szymczak, Inorg. Mater. **39**, 1092 (2003).
[24] J. Rodriguez-Carvajal, Physica B (Amsterdam) **192**, 55 (1993).
[25] H. T. Stokes and D. M. Hatch, ISOTROPY, http://stokes.byu.edu/isotropy.html, 2002.
[26] A. Le Bail, H. Duroy, and J. L. Fourquet, Mater. Res. Bull. **23**, 447 (1988).
[27] S. Streule, A. Podlesnyak, J. Mesot, M. Medarde, K. Conder, E. Pomjakushina, E. Mitberg, and V. Kozhevnikov, J. Phys.: Condens. Matter **17**, 3317 (2005).
[28] K. Conder, E. Pomjakushina, A. Soldatov, and E. Mitberg, Mater. Res. Bull. **40**, 257 (2005).
[29] A. A. Taskin, A. N. Lavrov, and Y. Ando, Phys. Rev. Lett. **90**, 227201 (2003).
[30] A. A. Taskin, A. N. Lavrov, and Y. Ando, Phys. Rev. B **71**, 134414 (2005).
[31] D. D. Khalyavin, S. N. Barilo, S. V. Shiryaev, G. L. Bychkov, I. O. Troyanchuk, A. Furrer, P. Allenspach, H. Szymczak, and R. Szymczak, Phys. Rev. B **67**, 214421 (2003).
[32] M. Baran, V. I. Gatalskaya, R. Szymczas, S. V. Shiryaev, S. N. Barilo, K. Piotrowski, G. L. Bychkov, and H. Szymczak, J. Phys.: Condens. Matter **15**, 8853 (2003).
[33] M. Baran, V. I. Gatalskaya, R. Szymczak, S. V. Shiryaev, S. N. Barilo, G. L. Bychkov, and H. Szymczak, J. Phys.: Condens. Matter **17**, 5613 (2005).
[34] Z. X. Zhou, S. McCall, C. S. Alexander, J. E. Crow, P. Schlottmann, S. N. Barilo, S. V. Shiryaev, G. L. Bychkov, and R. P. Guertin, Phys. Rev. B **70**, 024425 (2004).
[35] Z. X. Zhou and P. Schlottmann, Phys. Rev. B **71**, 174401 (2005).
[36] R. Caciuffo, D. Rinaldi, G. Barucca, J. Mira, J. Rivas, M. A. Señarís-Rodríguez, P. G. Radaelli, D. Fiorani, and J. B. Goodenough, Phys. Rev. B **59**, 1068 (1999).
[37] P. L. Kuhns, M. J. R. Hoch, W. G. Moulton, A. P. Reyes, J. Wu, and C. Leighton, Phys. Rev. Lett. **91**, 127202 (2003).
[38] D. Phelan, Despina Louca, K. Kamazawa, S.-H. Lee, S. Rosenkranz, M. F. Hundley, J. F. Mitchell, Y. Motome, S. N. Ancona, and Y. Moritomo, Phys. Rev. Lett. **97**, 235501 (2006).